Article

Decreasing trend in destructive potential of tropical cyclones in the South Indian Ocean since the mid-1990s

Check for updates

Shifei Tu [1,2,3], Zhenzhen Hu[1,2], Mei Liang[1,2], Wen Zhou [4,5] ✉, Johnny C. L. Chan [6,7,8] & Jianjun Xu [1,3] ✉

Tropical cyclone activity often leads to many adverse impacts and assessing their destructiveness is a crucial scientific concern. Here we investigated changes in the destructiveness of tropical cyclones worldwide using the power dissipation index and found that there is no clear trend in most basins, but a significant decrease in power dissipation index has been detected in the South Indian Ocean basin since 1994, which is almost entirely due to a decrease in both tropical cyclone frequency and duration in this basin. The decrease in tropical cyclone frequency is influenced by increased atmospheric stability. The decrease in tropical cyclone duration can be attributed to the changes in tropical cyclone locations. In addition, the weakened subtropical high is only observed in the South Indian Ocean (i.e., the Mascarene High), which is also associated with the decrease in tropical cyclone destructiveness. These findings have implications for assessing the destructive potential of future tropical cyclones.

Tropical cyclones (TCs) are one of the most frequent and destructive weather systems on earth, which can cause severe damage to infrastructure and ecosystems and even threaten human life and property, especially in underdeveloped coastal countries and regions[1–3]. According to a World Meteorological Organization (WMO) report[4], in the last 50 years (1970-2019), there have been 1,945 records of disaster events related to TC activity, resulting in 779,324 deaths and US\$1.4 trillion in economic losses. In general, the economic and property losses caused by landfalling TCs in developed countries are much greater than those in developing and underdeveloped countries, but the numbers of casualties caused by TCs in underdeveloped countries and regions are the reverse. In addition, TC-related disasters and economic losses have increased significantly in recent decades[4].

Therefore, the enormous harmful human toll of TC activity cannot be ignored. Assessing the destructiveness of TCs is crucial to reducing financial losses and human casualties worldwide[5,6]. Early studies[7,8] typically measured TC activity using a single indicator (such as TC intensity or frequency), but these indicators have limitations in assessing the destructiveness (or damage) of TC activity. To better reflect changes in TC activity, Emanuel[9] proposed a power dissipation index (PDI) to assess the destructiveness of TC activity, which combines TC intensity, duration, and frequency[10]. This index has been widely applied in subsequent studies[2,11–19]. How the

destructiveness of TCs will change under a warmer climate is a key scientific question of widespread interest. Many studies have been conducted to investigate the destructiveness of TCs at the global and basin scales, respectively. For example, since the mid-1970s, the destructiveness (PDI) of TCs has shown a significant increasing trend in both the Western North Pacific and the North Atlantic[9]. Using another widely used index, the Accumulated Cyclone Energy (ACE), Maue[20] found that the destructiveness of global TCs has undergone significant fluctuations, reaching its lowest level since 1977 in 2011. These changes are consistent with major shifts in Pacific climate. Lin & Chan[12] and Tu et al.[14] found that the Western North Pacific PDI decreased in 1993-2012 and increased in 1998-2016, respectively; these results also reflect the variability of TC activity on interdecadal scales. A previous work suggested that a slight increase in the destructiveness of TCs is detected in South Indian Ocean (SIO), which contributes to the increase in the frequency of intense TCs[21].

Because TC activity requires adequate heat content from the upper ocean, studies have suggested that TC activity is strongly influenced by upper-ocean thermal conditions and that the destructiveness of TCs is strongly correlated with increasing sea surface temperature (SST)[9,22], and many climate model simulations have shown similar results[23]. However, some studies have found that local SST cannot explain the variability in the destructiveness of TCs[24,25]. For example, there is no significant positive

[1]CMA-GDOU Joint Laboratory for Marine Meteorology & South China Sea Institute of Marine Meteorology, Guangdong Ocean University, Zhanjiang, China. [2]College of Ocean and Meteorology, Guangdong Ocean University, Zhanjiang, China. [3]Shenzhen Institute of Guangdong Ocean University, Shenzhen, China. [4]Key Laboratory of Polar Atmosphere-ocean-ice System for Weather and Climate, Ministry of Education, Department of Atmospheric and Oceanic Sciences & Institute of Atmospheric Sciences, Fudan University, Shanghai, China. [5]Key Laboratory for Polar Science of the MNR, Polar Research Institute of China, Shanghai, China. [6]School of Energy and Environment, City University of Hong Kong, Hong Kong, China. [7]Shanghai Typhoon Institute, China Meteorological Administration, Shanghai, China. [8]Asia-Pacific Typhoon Collaborative Research Center, Shanghai, China. ✉e-mail: wen_zhou@fudan.edu.cn; jxu@gdou.edu.cn

1

correlation between local upper-ocean heat content and TC destructiveness[14]. In fact, TC activity is more strongly related to changes in relative SST[26].

Due to the limitations of observational technology in earlier periods, the trajectory and intensity of TCs have large uncertainties. Satellites have monitored global TC activity since 1982, improving the uncertainties in the best-track dataset significantly[27,28]. Therefore, in this paper, we use historical best-track TC data from 1982 to 2021 to re-examine changes in the climatic tendency of the destructiveness of global TCs (the sum of the cubes of TC intensity). The results indicate that only the SIO has shown a clear downward trend in the destructiveness of TCs since the mid-1990s, while no significant downward trend has been observed in other TC basins. This decrease in the destructiveness of TCs in the SIO is due mainly to the decrease in TC frequency and duration.

Results
Observed trends in the PDI

Based on integration of the TC intensity cube, the average annual cumulative PDI of global TCs is 19.24×10^{11} m^3 s^{-2}, 14.33×10^{11} m^3 s^{-2}, and 4.90×10^{11} m^3 s^{-2} for the Northern Hemisphere and Southern Hemisphere, accounting for about three-quarters and one-quarter of global TC destructiveness, respectively. According to the time series, global TC destructiveness shows significant interannual variability (Fig. 1 and Supplementary Fig. 1), which is consistent with previous studies[29,30]. Overall, the annual cumulative PDI of TCs reaches its maximum in the 1990s, followed by a slight decreasing trend. The annual cumulative PDI in the Southern Hemisphere has decreased significantly since the mid-1990s (Supplementary Fig. 1c), while the PDI in the Northern Hemisphere decreases to a lesser extent and shows strong interdecadal variability throughout the study period (Supplementary Fig. 1b). The decrease in the destructiveness of TCs since the mid-1990s is consistent with previous results[20]. Furthermore, at the basin scale, except for obvious interannual and interdecadal variations, only the annual cumulative PDI of the SIO has a significant abrupt change of linear trend detected in the mid-1990s and shows a clear downward trend thereafter (Fig. 1).

ACE index also shows the same downward trend since the mid-1990s (Supplementary Fig. 2).

We first examine the characteristics of the destructiveness in the SIO basin. The statistical results show that the average annual cumulative PDI in the SIO is 3.12×10^{11} m^3 s^{-2}. The time series of the cumulative PDI (Supplementary Fig. 1g) shows clear interannual and interdecadal variability. The maximum cumulative PDI occurs in 1994 (6.46×10^{11} m^3 s^{-2}), which is seven times higher than the minimum in 1987 (0.86×10^{11} m^3 s^{-2}). The cumulative PDI increases gradually but reaches the maximum rapidly in 1994 and then decreases significantly (the downward trend reaches the 95% confidence level), with a linear trend of -0.72×10^{11} m^3 s^{-2} per decade (Fig. 2a, P = 0.03). Based on this linear trend, the cumulative PDI decreases by about 45% at the end of the 1994–2021 period. Tridaiana & Marzuki[21] showed an increase in PDI and ACE indices in the SIO region, which differs from the present study because they considered only TCs with categories 1–5, while tropical depressions and tropical storms were not considered. For comparative analysis, we divide this downward period (1994-2021) into two sub-periods (i.e., P1: 1994-2007 and P2: 2008-2021). In P1, the cumulative PDI in the SIO basin is 3.93×10^{11} m^3 s^{-2} (Table 1), while it decreases to 2.82×10^{11} m^3 s^{-2} in P2, ~28% less than in P1, which means that the destructiveness of TCs in the SIO decreases by more than a quarter in P2. Over the same period, the quantitative results for ACE also show a linear trend of -15.8×10^4 m^2 s^{-2} per decade (Supplementary Fig. 2g, P = 0.01) and a 27% difference between P1 and P2.

These phenomena are significantly different from those in other TC basins (Fig. 1). We counted the evolution of the cumulative PDI in different TC basins during the period 1982-2021, but we detected no significant upward or downward trend in TC destructiveness. A slight downward trend (P = 0.22) in the cumulative PDI can be found only in the Western North Pacific basin. This change is likely related to the abrupt interdecadal change in the PDI in 1998[12,14]. In the Eastern North Pacific basin, the cumulative PDI of TCs abruptly decreases after 1995, while in the North Atlantic, it abruptly increases after 1995, both without a significant upward or downward trend. In addition, the cumulative PDI in the South Pacific basin does not show any significant trend over the period 1994-2021. Therefore, the decrease in
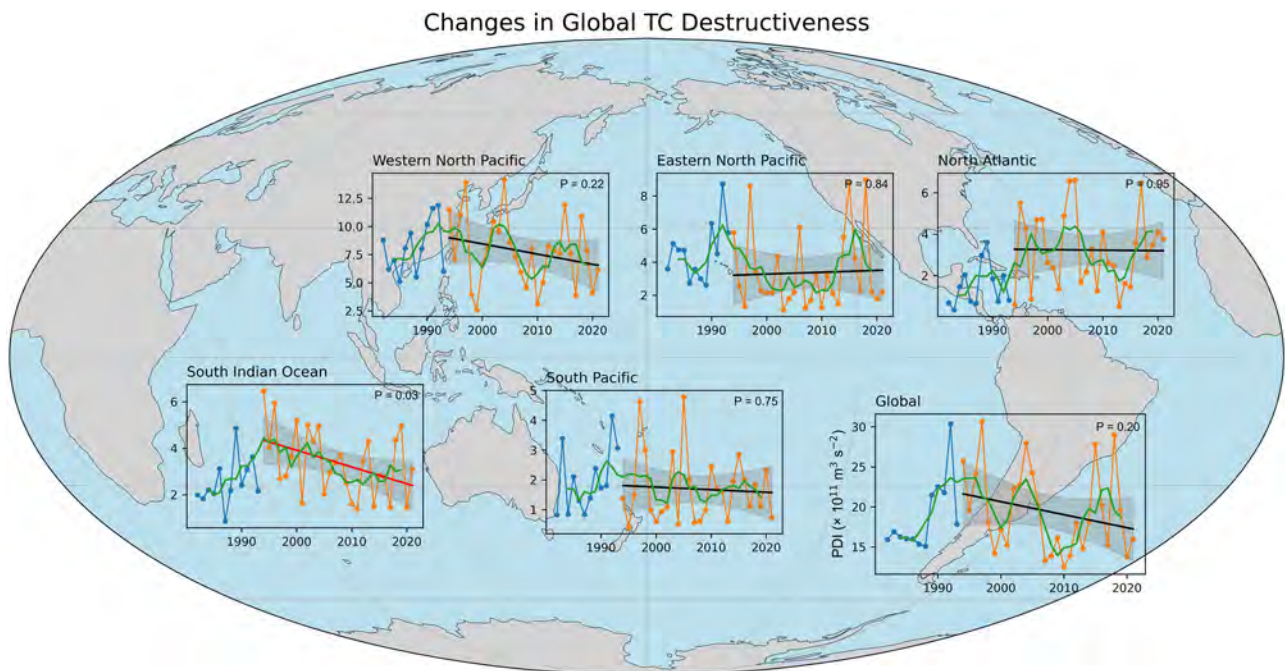

Fig. 1 | Time series of the cumulative power dissipation index (PDI) of tropical cyclones (TCs) for each basin and the global. Shaded areas are the two-sided interval of the linear trend at the 95% confidence level; the solid line (red is significant) represents the linear regression since the mid-1990s. The green curve represents the 5-year running average distributions of the PDI.
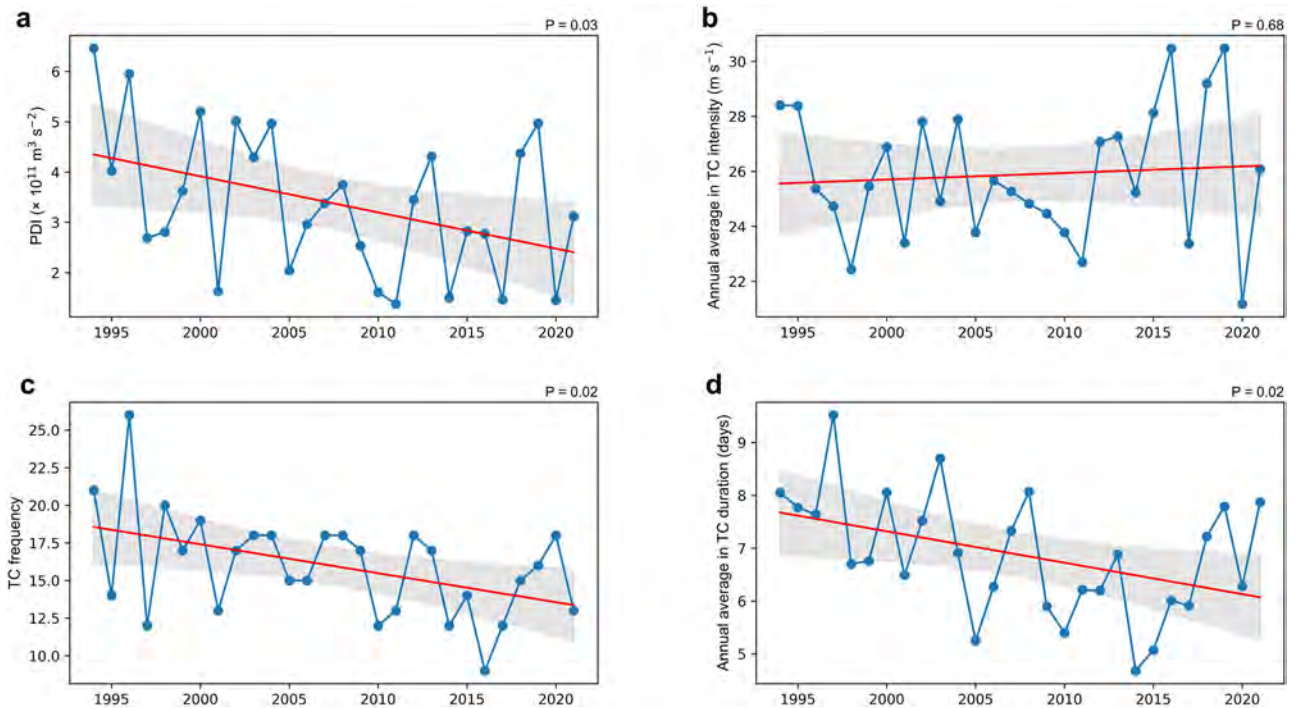
Fig. 2 | Time series of SIO TC-related parameters during the period 1994-2021. a PDI, **b** TC intensity. **c** TC frequency. **d** TC duration. Shaded areas are the two-sided interval of the linear trend at the 95% confidence level; red lines are the linear regression.

Table 1 | Differences in the cumulative PDI of TCs and their contributors in the SIO between periods P1 (1994–2007) and P2 (2008–2021)

	PDI (×10^{11} m^3s^{-2})	Intensity (m s^{-1})	Duration (day)	Frequency	TC days (day)
Climatology	3.12	25.64	6.83	16.05	109.17
P1	3.93	25.90	7.38	17.36	126.14
P2	2.81	26.00	6.46	14.57	92.20
Difference	–1.12	0.10	–0.92	–2.79	–33.95
Percent	–28.50	0.38	–12.50	–16.07	–26.91
P-value	0.04	0.59	<0.01	0.03	<0.01

the PDI in the Southern Hemisphere can be attributed mainly to the change in the PDI in the SIO. However, it remains unclear why the cumulative PDI is decreasing significantly only in the SIO basin.

Changes in PDI-related contributors in SIO

According to the definition of the cumulative PDI[9,10], TC frequency, duration, and intensity are the three contributors to changes in the PDI, so we analyze the characteristics of these three factors. The statistical results show that the average TC intensity over the SIO is 25.64 m s^{-1}, the TC frequency is 16.05 per year, and the average TC duration is 6.83 days (Table 1). The time series of these three factors also show obvious interannual variations (Fig. 2b–d). Among them, the average TC intensity shows a slightly increasing trend (P = 0.68) during the period 1994-2021 (Fig. 2b), while the TC frequency and the average TC duration decrease significantly during the same period (Fig. 2c, d, P = 0.02). Therefore, the significant downward trend in the cumulative PDI from 1994 to 2021 is mainly caused by the decrease in TC frequency and duration. Combined with a previous study[21], the increase in the frequency of strong TCs has contributed to the fact that there has been no decrease in the mean intensity (Fig. 2b). The decrease in TC frequency is predictable, and it has also been noted in previous studies[31,32] that global

warming will lead to a decrease in TC frequency in the SIO, and while this may be beneficial in terms of reducing flooding, it will also allow for a decrease in precipitation in Southeast Africa, which could have negative impacts on agriculture.

In order to better quantify the changes in TC activity status in the SIO basin, we also calculate the differences in these variables between P1 (1994-2007) and P2 (2008-2021). As shown in Table 1, the average intensity in these two sub-periods is 29.90 and 26.00 m s^{-1}, respectively, an increase of <1% during P2 (P = 0.59). TC frequency decreases from 17.36 to 14.57, a difference of 2.79 TCs (16%, P = 0.03). The downward trend in TC frequency observed here is consistent with previous work and is likely related to the weakened tropical circulations associated with increased atmospheric stability[23,33,34]. The result shows that TC duration in P2 changes from 7.38 days in P1 to 6.46 days, with a difference of 0.92 day (13%, P < 0.01). TC days, simply defined as TC frequency multiplied by average TC duration, can also be used to characterize the activity of TCs in each TC basin[22,35]. The average TC days in the SIO are 33.95 days less in P2 (27%, P < 0.01) than in P1. The magnitude of this change is comparable to the downward trend of the cumulative PDI between these two subperiods, while the slightly increasing trend in TC intensity makes a negligible contribution to the change in the PDI over the SIO basin.

We have also examined these changes in PDI contributors in other TC basins, but except for the Western North Pacific, these other TC basins show no apparent changes in TC intensity and TC days (Supplementary Figs. 3-4). The relationship between the decreased cumulative PDI and its contributors in the SIO is similar to the changes in the Western North Pacific from 1993 to 2012[12], where the decreased PDI is also influenced by changes in TC frequency and duration. However, the decreased PDI in the Western North Pacific during 1993-2012 is only part of the interdecadal variability, as a significant upward trend can be found during the period 1998-2016, and this change is associated with a gradual increase in TC intensity[14]. However, the cumulative PDI in the SIO basin has not yet shown a significant upward tendency. Are the changes in the destructiveness of TCs in the SIO and Western North Pacific basins, and the possible reasons for them, consistent?
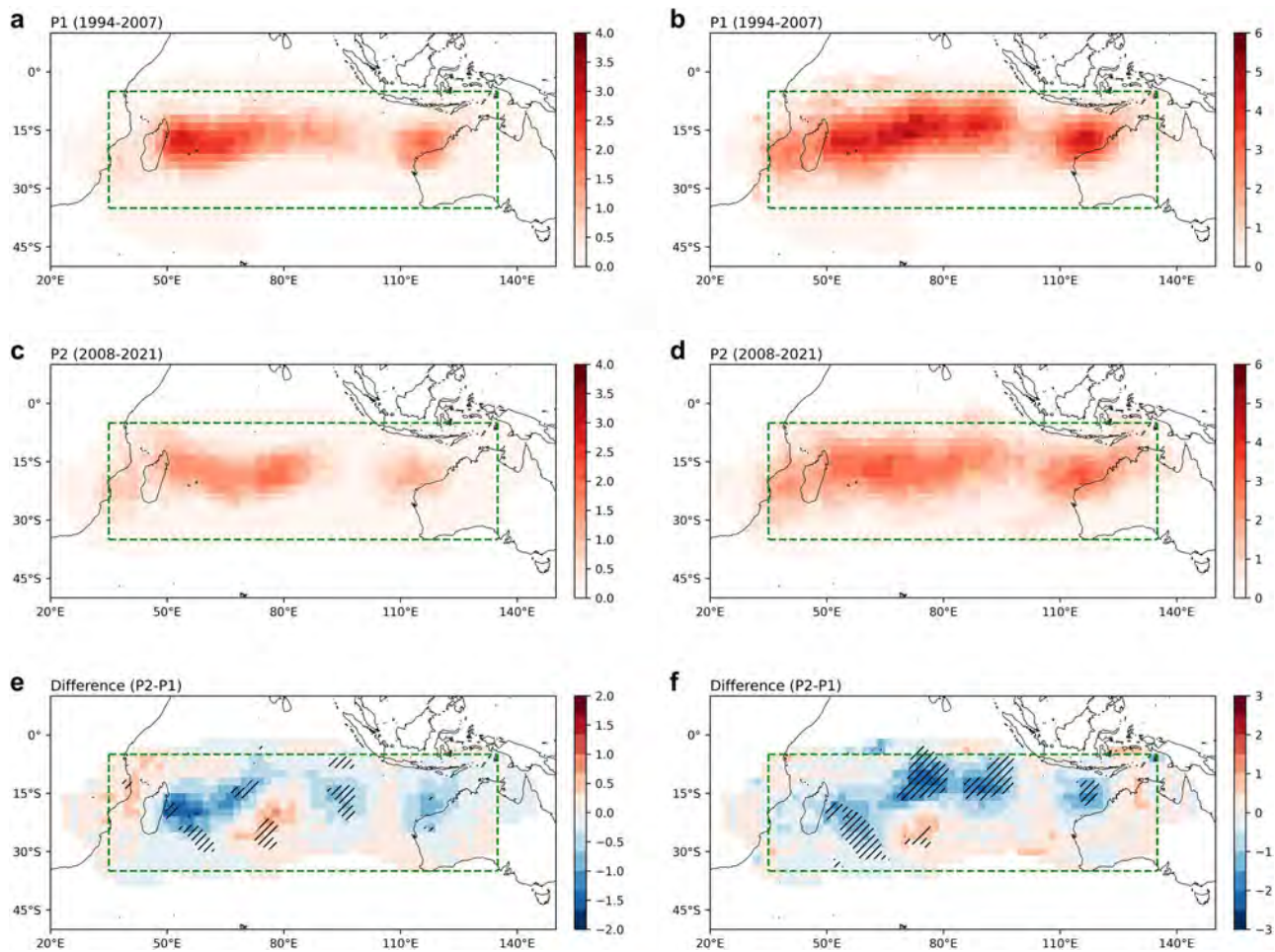
Fig. 3 | Distribution of the regional PDI and track density. a regional PDI ($\times 10^9 \, \text{m}^3 \, \text{s}^{-2}$ per grid) in P1. **b** track density (times per grid) in P1. **c, d** same as **a, b**, but for P2. **e, f** same as **a, b** but for the difference between P1 and P2. Dashed areas indicate differences significant at the 95% confidence level. The green dashed rectangle represents the main TC area of the SIO.

Changes in the track and movement of TCs

In the analysis above, we have investigated the evolution of the time series of the PDI and its contributors, and their spatial variation is of further interest here. According to the regional PDI distribution (in a 2°×2° grid; see Methods), it is observed that TC destructiveness in P1 is concentrated mainly east of Madagascar and northwest of Australia, while the destructiveness in both these regions is significantly weakened in the later subperiod, and the maximum value appears in the central region of the SIO near 80°E. These changes can be clearly detected from the distribution of differences in the regional PDI (Fig. 3). The regional PDI can be determined from the average regional TC intensity and TC track density. Despite some TC intensification along the eastern coast of Africa and around 80°E and 110°E in the SIO, other regions of the SIO do not change significantly, implying that the contribution of regional TC intensity to regional PDI change is almost negligible. Therefore, changes in TC track density contribute the majority of the regional PDI variation.

Furthermore, we analyze the average positions of TC activity in the SIO during P1 and P2. Supplementary Table 1 and Supplementary Fig. 5 shows the change in TC positions, where the average position of TC activity in P1 is 15.71°S, 79.97°E, but in P2 it is 16.52°S, 80.59°E, which shows a significant southward shift compared to P1 ($P < 0.01$). The mean TC genesis position also shows a significant southward shift in P2 ($P = 0.03$). Previous studies have found a significant poleward migration of global TCs[36–38], which is likely to be influenced by tropical expansion[34,39,40]. Our results also show that TC activity in the SIO appears to undergo a poleward migration during P2. However, a significant westward shift in the location of TC generation[41] is not detected in 1994-2021 (i.e., only a slight change in our result, $P = 0.14$), most likely due to the selection of a different study period.

In general, TCs are generated in the lower latitudes of the tropics and then gradually transported westward and poleward under the influence of the steering flow and the beta effect[42,43]. However, the westward component is stronger in the early phase under the equatorial easterlies, while the beta effect gradually increases with increasing latitude. The distribution of TC tracks (Fig. 4) indicates that TCs migrate more westward in P1. However, in P2, the westward migration of TCs is not as obvious as in P1, and the distribution of TC tracks is relatively more dispersed. Is it possible that TC tracks change significantly in these two sub-periods?

TCs across the SIO basin are possibly to be drove by the large-scale zonal flow[44], so it is important to understand the spanning distance of the TC westward. In this study, we calculate the longitude differences of each TC from its genesis position to its westernmost position over its entire lifetime to explore changes in the distance of TC westward migration. Based on the time series, the westward distance of TCs in the SIO gradually decreases from 1994 to 2021, with a linear trend of 2.20° longitude per decade ($P = 0.03$; Fig. 5a). In P1, the westward distance of TCs is 12.95° longitude (Supplementary Table 1), while in P2 it is 9.04° longitude, with a decrease of 3.9° longitude (30%, $P < 0.01$).

In addition, a similar feature can be found in the time series of the average direction of TC activity (Fig. 5b). The results show a significant decreasing trend in the average direction of TC activity in the SIO during 1994-2021, with a linear trend of 5.85° per decade (P = 0.04); i.e., the composite TC translation direction gradually shifts from west to south.
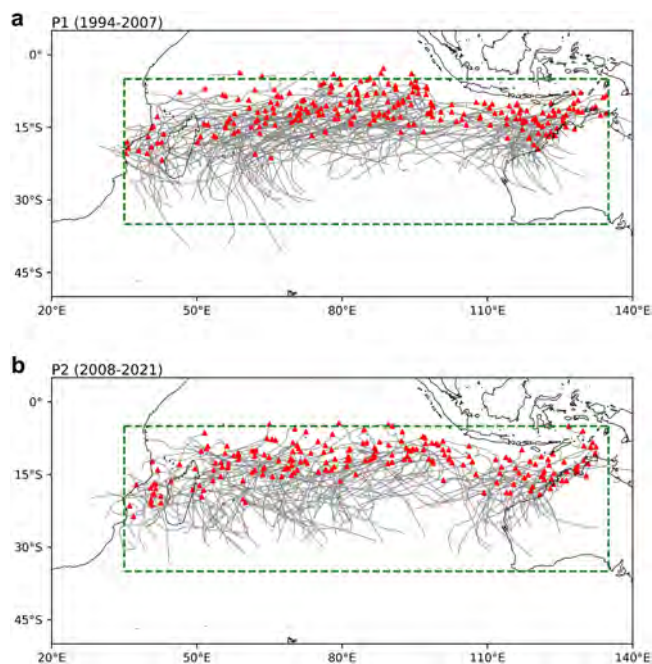
Fig. 4 | Distribution of TC tracks during P1 and P2. a P1 (1994-2007). **b** P2 (2008-2021). Red triangles are the genesis positions of TCs, and gray curves are the trajectory of TCs. The green dashed rectangle represents the main TC area of the SIO.
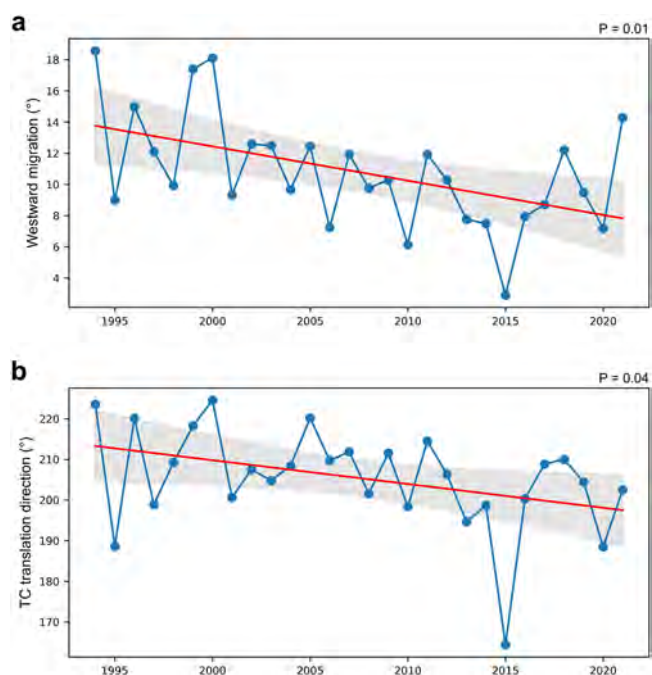

Fig. 5 | Time series of SIO TC-related locations and directions during the period 1994–2021. a Distance of TC westward migration (longitude). **b** TC translation direction. Shaded areas are the two-sided interval of the linear trend at the 95% confidence level; red lines are the linear regression.

Furthermore, the average direction of TC activity in P1 is 211.74° (i.e., northward is 0° and clockwise is positive, Supplementary Table 1), while the average direction of TC activity in the SIO in P2 is 200.77°, a difference of 10.97° ($P < 0.01$). Therefore, the average translation direction of TCs in P2 is more southward than in P1.

Therefore, according to the statistical results of the locations and tracks of TC activity, TCs appear to be generated more westward in P2

(insignificant), but the distance of westward migration is significantly reduced. TC generation location is southward and thus the beta effect is enhanced, which may cause TCs to be deflected southward to higher latitudes earlier, and thus TC is weaken and disappear faster. Meanwhile, this study also found that the distance of TC southward migration remains unchanged (Supplementary Table 1 and Supplementary Fig. 5c), thus the trajectory of TCs is also significantly shortened. Since TC trajectories can be determined by translation speed and TC duration, the statistics show that the average TC translation speed in the SIO has not decreased (Supplementary Table 1), so the downward trend in TC duration is caused mainly by the gradually shortened TC trajectory. However, characteristics of TC activity that are similar to those in the SIO (such as the westward migration of the genesis site and the shortening of the TC trajectory) are not found in the other TC basins.

Possible mechanism of influence

Based on the above analysis, we know that changes in TC frequency and track distribution contribute significantly to the decreasing PDI in the SIO. So, what causes the changes in TC frequency and tracks?

The influence of environmental thermodynamic conditions is considered in order to explore a possible mechanism of influence. Previous studies have suggested that TC intensity may increase with global warming, especially TCs in the more intense categories[22,45,46]. First, thermal conditions such as SST and water vapor content are sufficiently favorable for TC activity (Fig. 6a, b), as well as TC heat potential (Supplementary Fig. 6), allowing TC intensity to be maintained. Malan et al.[47] show that the increase in TCHP favors an increase in severe storms, but the TC frequency decreases during the same period, a discrepancy associated with increased atmospheric anticyclones in the SIO. Our results also suggest that the atmospheric dynamical conditions in the SIO region are not favorable for TC activity. Specifically, compared to P1, the atmospheric stability between the upper and lower layers over the SIO region is significantly enhanced during P2 (Fig. 6c), which is likely the main reason for the significant decrease in the frequency of TC generation during the 1994-2021 period. This increase in atmospheric stability will suppress atmospheric convection and decrease upward mass flux in the tropics and subtropics[23,33,34]. Under such conditions, it is discovered that the CAPE (convective available potential energy) in the SIO region is also found to be significantly decreased (Fig. 6d), resulting in a decrease in TC generation.

On the other hand, TC trajectories and intensities are influenced by the subtropical high[48], the subtropical high around the SIO (i.e., Mascarene High, MH) can regulate TC tracks through the steering flow (a counterclockwise rotating flow around the MH). Our investigation found that the atmospheric geopotential height at 850 hPa is weakened significantly during P2 (Fig. 6e), especially over the western MH, which implies a weakened MH. This is also evident from the 1540 isopotential line during P1 and P2 (Fig. 6f). Because the Southern Hemisphere subtropical high behaves as a counterclockwise rotating system, the reduction in the MH means that the counterclockwise rotation is weakened, which can lead to a clockwise wind difference around the MH.

We know that TC motion is usually caused by a combination of the steering flow and the beta effect. Relatively, except when the translation speed of a TC is very small, the influence of the steering flow on TC motion is stronger than that of the beta effect[49]. Since TC trajectories in the SIO are strongly influenced by the counterclockwise steering flow around the periphery of the MH, the clockwise wind difference around the MH implies that the TC steering flow is weakened in the SIO region. A clear westerly and southwesterly wind difference is presented in the lower-latitude area around the island of Madagascar and its southeastern waters combined with the southward shift of TC genesis locations, thus increasing the relative contribution of the beta effect. This process is conducive to shortening the westward migration distance of TCs, thus shifting the translation direction of TCs to the south earlier, and finally producing shortened TC tracks and durations.
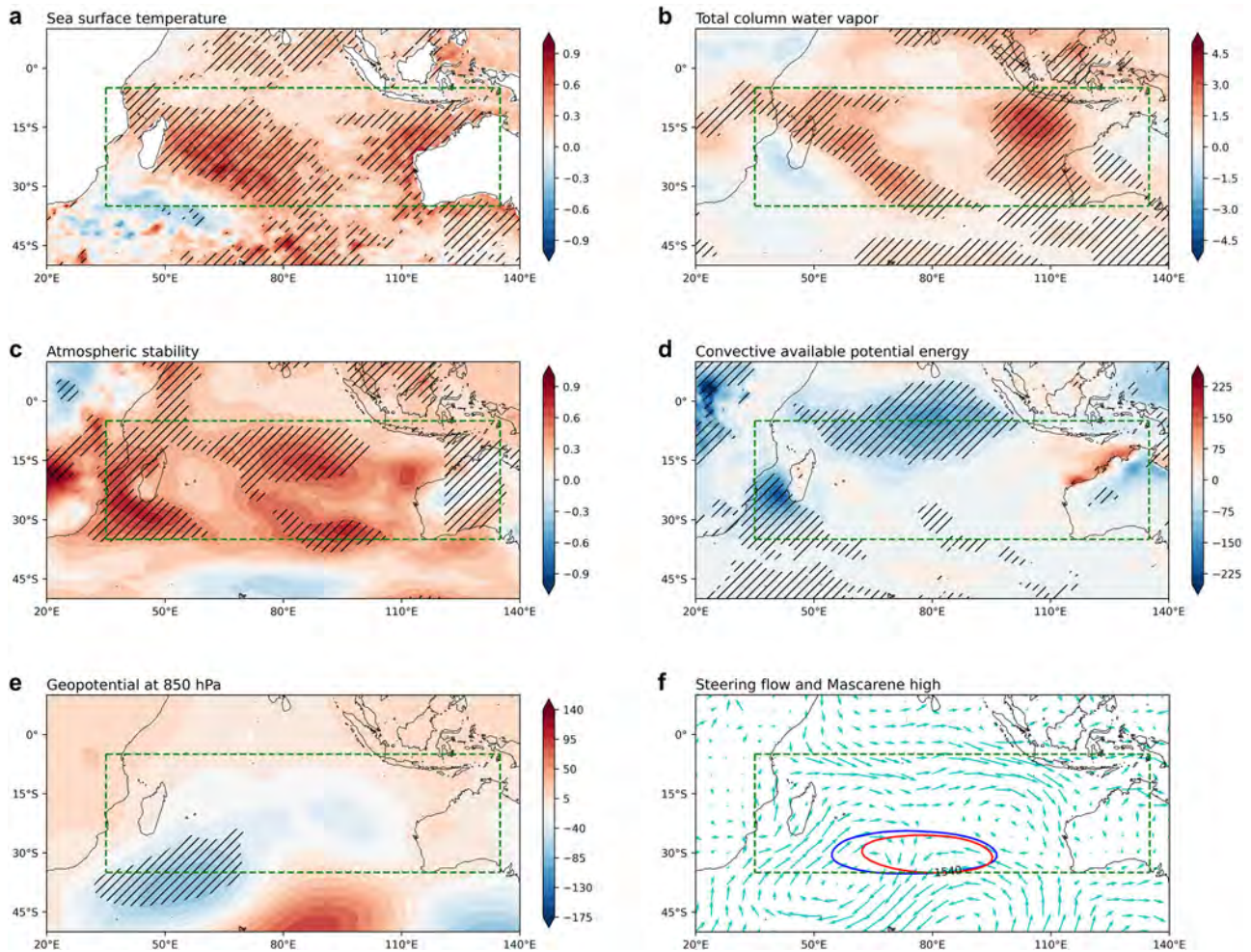
Fig. 6 | Differences in various TC thermodynamic conditions. a Sea surface temperature. **b** Total column water vapor. **c** Atmospheric stability. **d** Convective available potential energy. **e** Geopotential at 850 hPa. Dashed areas in subplots **a**–**e** indicate differences that are significant at the 95% confidence level. **f** Steering flow and Mascarene High distributions; blue and red curves represent the 1540 gpm isopotential line at 850 hPa. These influence factors are calculated as the average from November to April. The green dashed rectangle represents the main TC area of the SIO.

The decrease in the MH plays an important role in the decrease in TC destructiveness. However, a similar phenomenon has not been observed in any other major TC basin (Supplementary Fig. 7), and some studies have even found a significant intensification of the subtropical high in the Western North Pacific basin, which may also affect TC activity[12,50,51]. The weakening of the subtropical high seems to occur only in the SIO, while the geopotential increases significantly in the other TC basins. This means that the differences in the SIO subtropical high and TC changes are significant compared to the other basins, causing the trend in the destructiveness of TCs in the SIO to be inconsistent with that in the other TC basins. However, the exact cause of this incongruence is unclear and requires further research.

Discussion

In this study, we found that the destructiveness of TCs in the SIO decreases significantly during the period 1994-2021, mainly due to the decrease in TC frequency and duration. Consistent with the results of many previous studies, the decrease in TC frequency is likely due to the decrease in upward mass flux over the tropics[23,33,34], which may be related to the strength of atmospheric stability under a warming climate. The decrease in TC duration implies that it is mainly due to the shortening of TC tracks. This is because the change in TC translation speed between the two periods is small. The most direct cause of the shortening of TC tracks is the significant weakening of the MH, which weakens the steering flow around it and correspondingly strengthens the contribution of the beta effect. As a result, TCs deviate and enter higher latitudes earlier, then weaken and disappear faster. We found

that the weakening of the MH has had a significant impact on TC activity in recent decades, and future research should focus on the impact of these changes on TC activity. Additionally, the cumulative PDI in the other TC basins has not decreased significantly, probably related to the unweakened subtropical high in these basins (Supplementary Fig. 7).

Previous studies have found that PDI in the SIO has increased in recent decades[18,21,52], which differs from the decrease in PDI since the mid-1990s found in this study due to the different TC samples considered. In terms of spatial distribution, the decrease in PDI is associated with a decrease in TC track density at low latitudes, northwest Australia, and in the waters east of Madagascar (Fig. 3). This implies a decrease in the number of TCs landing in northwest Australia and near the Madagascar islands during the P2 period. In fact, since the 1980s, the frequency of intense TCs in the SIO has increased, especially the frequency of category 5 level TCs[52,53], which is a result of global warming. This phenomenon has been found in other relevant studies[54,55]. While the frequency of tropical storms has decreased slightly, the frequency of TC genesis and landfall has also decreased in the Southwest Indian Ocean (SWIO)[56]. This study supports similar findings for TC frequency, but there has been no significant change in average intensity, which is possible because the contributions of intense and weak TCs offset each other. The average TC intensity shows a clear increase in magnitude over the last decade (Fig. 2b), suggesting a more pronounced increase in the proportion of intense TCs and potentially posing a challenge to tropical cyclone forecasting in the region. However, the regional PDI is not uniformly weakened, and this study found a slight increase in TC destructiveness along the southeast coast of Africa

during P2 (Fig. 3e), which is likely related to the westward shift in the location of TC generation in SWIO[41].

The decrease in the PDI since the mid-1990s and its possible causes were examined in this study. If we further examine the time series of PDI and find an increasing trend between 1982 and 1993, what is the reason? As shown in Supplementary Fig. 8, the increase in average TC intensity and duration contribute to the changes in PDI during this period. Because the average distance of TCs to land is gradually increased during 1982-1993, indicating a longer duration of TC activity at sea (Supplementary Fig. 9a, b). The warm ocean surface provided an amount of energy that then led to an increase in the average TC intensity. In contrast, environmental factors do not change significantly during the same period and thus have a negligible influence on the destructiveness of SIO TCs. The changes in the PDI before 1994 are mainly due to an increase in the average TC intensity, which is associated with an increase in the duration of TCs over water. During the same period, the overall PDI on land also weakened, associated with a decrease in the frequency of landfalling TCs, but there was no significant change in the PDI of individual TCs on land, and the average duration on land decreased slightly (Supplementary Fig. 9). Since 1994, our results show that both the total PDI on land and that of individual TCs have decreased, but there has been no significant change in the distance from land over the same period (Supplementary Fig. 10). However, the duration offshore has decreased significantly, which may be related to the poleward shift in the trajectory of TCs (Fig. 5 and Supplementary Fig. 5). This explains the different variations in PDI changes before and after 1994. In addition, the frequency of TC landfalls has decreased slightly, and the onshore duration has remained largely unchanged (Supplementary Fig. 10). We have discussed the different trends in PDI before and after 1994, as well as its changes over land. These features reflect the large-scale interdecadal variability characteristics of PDI in the SIO, and it is worth continuing to focus on whether the decreasing PDI will gradually turn into an increasing trend in the future.

Many studies have also analyzed the relationship between climate indices and TC activity in the SIO (or SWIO). On interannual time scales, the El Niño-Southern Oscillation is considered important for TC generation and trajectory in the SIO[57–59]. El Niño-Southern Oscillation can modulate the large-scale environmental field changes associated with TC generation; the decrease in TC frequency in the SWIO during a strong El Niño is associated with changes in large-scale thermodynamic parameters, in which case the equatorward movement of the subtropical jet offsets the effects of tropospheric humidity and SST on TCs, which in turn suppresses TC activity[60]. Chikoore et al.[61] identified La Niña events and anomalous easterly circulation associated with SWIO SSTs as one of the mechanisms supporting TC generation in the Mozambique Channel. A previous study[53] suggests that there is significant interannual variability in the frequency of TC landfalls in Madagascar and Mozambique, which is influenced by the El Niño-Southern Oscillation and the Quasi-Biennial Oscillation. The Antarctic Oscillation can also influence TC activity in the SIO, which increases by 50% to 100% in northwest Australia when the Antarctic Oscillation is in positive phase due to enhanced water vapor convergence and upward motion[62]. In addition, the Madden-Julian Oscillation has been shown to exert a significant influence on SIO TCs, particularly over the northwest coast of Australia[59,63]; TCs in the SIO are also associated with localized Indian Ocean Dipole phenomena[64,65]. These features reflect the interaction between climate oscillations and TC occurrence[66]. In particular, whether the currently observed weakening of TC destructiveness in the SIO causes a change in the correlation between TC activity and these large-scale climate oscillations is also a question that needs to be further investigated.

Although the PDI in the SIO accounts for about 16% of the total global destructiveness, it is also an important part of global TC activity and has significant economic and social impacts on the eastern coast of Africa and the northwestern Australia[18,67]. Southern Hemisphere countries are more vulnerable to the destructive nature of tropical cyclones due to their lower adaptive capacity compared to Northern Hemisphere countries[68]. For example, Cyclone Idai in 2019 caused approximately 1,300 deaths, affected more than three million people, and caused \$2.2 billion in direct economic losses; Cyclone Freddy, an SIO-generated cyclone in 2023, broke the record for longest duration on earth[69]. Therefore, it is also important to be concerned and closely examine the changes in TC activity in the region, especially in relation to the inconsistencies (as in this study) with other TC basins under the current warming climate.

Methods

Data

The International Best Track Archive for Climate Stewardship-Joint Typhoon Warning Center (IBTrACS-JTWC) dataset[70] is widely used in tropical cyclone (TC) studies[20,26,41,71,72], which includes the 3-hour position (longitude and latitude), minimum sea level pressure, and maximum sustained wind speed near the TC center, etc. In this study, the records of non-TC systems (such as extratropical, wave, disturbance, and others) are excluded. All records with TC intensity greater than 12.35 m s^{-1} (~24 kt) are counted in this study.

In this paper, the fifth generation ECMWF (European Centre for Medium-Range Weather Forecasts) atmospheric reanalysis of the global climate (ERA5) dataset[73] and the EN4.2.2 ocean analysis dataset[74] obtained from Met Office Hadley Centre are used to investigate the possible environment factors contributing to TC activity.

Power dissipation index and TC-related parameters

In this paper, the power dissipation index (PDI)[9] is used to investigate changes in the destructiveness of TCs, defined as the sum of the cubes of the 3-hourly maximum sustained wind speed (TC intensity) over the lifetime of a TC; hence the cumulative PDI in a TC year is shown in Eq. (1):

$$PDI = \sum_{i=1}^{N} \int_0^\tau V_{\max}^3 \, dt \qquad (1)$$

It can be considered a combination of TC frequency, duration, and intensity. Changes in the PDI of TCs at the global, hemispheric, and basin scales are calculated separately, among which the data from five basins, namely the Western North Pacific, Eastern North Pacific, North Atlantic, South Indian Ocean, and South Pacific, are counted. Considering that most of the early records in the North Indian Ocean are "Not Reported" in the IBTrACS data, TCs in the NIO are excluded in the present study.

Regional changes in the PDI, TC intensity, and track density are also investigated in this work. These are counted in a 2° × 2° grid over the SIO. The regional PDI is defined similarly to the above formula, but for TC tracks entering each 2° × 2° grid. It is therefore mainly a result of regional TC intensity and TC track density. To better represent changes in the regional PDI, regional TC intensity, and TC track density, a 5×5 spatial grid filter is used here.

Similarly, Accumulated Cyclone Energy (ACE) index can also represent the destructiveness of TCs[20,21,29,55,72] which is defined as the sum of the square of TC intensity in a year shown in Eq. (2):

$$ACE = \sum_{i=1}^{N} \sum_{t=0}^{\tau} V_{\max}^2 \qquad (2)$$

ACE's contributors are the same as PDI. This work also calculates changes in ACE at the global, hemispheric, and five basin levels from the 3-hour interval best-track dataset (IBTrACS-JTWC).

Possible influence factors and environmental conditions

To investigate the changes in TC track in the SIO during the period 1994-2021, the distance of TC westward and southward migration is examined, the distance of TC westward migration is defined as the difference between the genesis and westernmost longitude for each TC. Similarly, the distance of TC southward migration is the difference between the genesis and southernmost latitude for each TC.

Environmental factors of influence, including SST, total column water vapor, relative humidity, atmospheric stability, convective available potential energy, geopotential, and steering flow, are obtained from the monthly ERA5 dataset. Referring to the previous method[34,75], atmospheric stability (AS) is defined as Eq. (3):

$$AS = \theta_{300} - \theta_{900} \qquad (3)$$

which represents the potential temperature difference between 300 and 900 hPa (θ_{300} and θ_{900}), respectively, in which the potential temperature is defined as:

$$\theta = T \left(\frac{P_0}{P} \right)^{\frac{R}{c_p}} \qquad (4)$$

where T in Eq. (4) is the absolute temperature (K), R is the gas constant of air, c_p represents the specific heat capacity at a constant pressure, P_0 and P are the reference pressure (usually taken as 1000 hPa) and atmospheric pressure, respectively. In general, $R/c_p = 0.286$ for the atmosphere.

TC heat potential (TCHP) represents the heat contained in the upper layer of the 26 °C isotherm of the upper ocean[17]. It is defined as:

$$TCHP = c_p \rho \int_{D_{26}}^{0} [T(z) - 26] dz \qquad (5)$$

In Eq. (5), c_p is the specific heat capacity at a constant pressure, usually taken as 4178 J kg^{-1} °C^{-1}; ρ is the density of sea water, taken as 1026 kg m^{-3} in the upper ocean; D_{26} is the depth of the 26 °C isotherm, and $T(z)$ is the in-situ temperature from the ocean analysis data in the EN4.2.2 ocean analysis dataset.

Data availability
TC best-track data are taken from the IBTrACS v4 dataset (https://www.ncdc.noaa.gov/ibtracs/). Environmental factors are taken from ERA5 reanalysis (https://cds.climate.copernicus.eu/cdsapp#!/home) and EN4.2 ocean analysis (https://hadleyserver.metoffice.gov.uk/en4/download-en4-2-2.html). Source data are provided with Figshare (https://doi.org/10.6084/m9.figshare.26706655).

Code availability
All Python codes used to generate the results are available on request from the first author (S.T., email: tusf@gdou.edu.cn).

References
1. Pielke, R. A. J., Rubiera, J., Landsea, C. W., Fernandez, M. L. & Klein, R. Hurricane vulnerability in Latin America and the Caribbean: Normalized damage and loss potentials. *Nat. Hazards Rev.* **4**, 101–114 (2003).
2. Zhang, Q., Wu, L. & Liu, Q. Tropical cyclone damages in China 1983–2006. *Bull. Am. Meteorol. Soc.* **90**, 489–496 (2009).
3. Peduzzi, P. et al. Global trends in tropical cyclone risk. *Nat. Clim. Change* **2**, 289–294 (2012).
4. World Meteorological Organization (WMO). Focus on tropical cyclones. in *Atlas of Mortality and Economic Losses from Weather, Climate and Water Extremes* (1970–2019). 62–65. (WMO publications, 2021).
5. Goldenberg, S. B., Landsea, C. W., Mestas-Nuñez, A. M. & Gray, W. M. The recent increase in Atlantic hurricane activity: causes and implications. *Science* **293**, 474–479 (2001).
6. Hsu, P. C., Chu, P. S., Murakami, H. & Zhao, X. An abrupt decrease in the late-season typhoon activity over the western North Pacific. *J. Clim.* **27**, 4296–4312 (2014).
7. Emanuel, K. A statistical analysis of tropical cyclone intensity. *Mon Weather Rev.* **128**, 1139–1152 (2000).
8. Landsea, C. W., Harper, B. A., Hoarau, K. & Knaff, J. A. Can we detect trends in extreme tropical cyclones? *Science* **313**, 452–454 (2006).
9. Emanuel, K. Increasing destructiveness of tropical cyclones over the past 30 years. *Nature* **436**, 686–688 (2005).
10. Emanuel, K. Environmental factors affecting tropical cyclone power dissipation. *J. Clim.* **20**, 5497–5509 (2007).
11. Vecchi, G. A., Swanson, K. L. & Soden, B. J. Whither hurricane activity? *Science* **322**, 687–689 (2008).
12. Lin, I. I. & Chan, J. C. Recent decrease in typhoon destructive potential and global warming implications. *Nat. Commun.* **6**, 7182 (2015).
13. Li, R. C., Zhou, W., Shun, C. M. & Lee, T. C. Change in destructiveness of landfalling tropical cyclones over China in recent decades. *J. Clim.* **30**, 3367–3379 (2017).
14. Tu, S., Xu, F. & Xu, J. Regime shift in the destructiveness of tropical cyclones over the western North Pacific. *Environ. Res. Lett.* **13**, 094021 (2018).
15. Sajjad, M., Li, Y., Li, Y., Chan, J. C. & Khalid, S. Integrating typhoon destructive potential and social-ecological systems toward resilient coastal communities. *Earth's. Future* **7**, 805–818 (2019).
16. Liu, L., Wang, Y., Zhan, R., Xu, J. & Duan, Y. Increasing destructive potential of landfalling tropical cyclones over China. *J. Clim.* **33**, 3731–3743 (2020).
17. Tu, S. et al. Differences in the destructiveness of tropical cyclones over the western North Pacific between slow-and rapid-transforming El Niño years. *Environ. Res. Lett.* **15**, 024014 (2020).
18. Vidya, P. J. et al. Increased cyclone destruction potential in the Southern Indian Ocean. *Environ. Res. Lett.* **16**, 014027 (2020).
19. Hsu, P. C. et al. Future changes in the frequency and destructiveness of landfalling tropical cyclones over east asia projected by high-resolution AGCMs. *Earth's Future* **9**, e2020EF001888 (2021).
20. Maue, R. N. Recent historically low global tropical cyclone activity. *Geophys. Res. Lett.* **38**, L14803 (2011).
21. Tridaiana, S. & Marzuki, M. Exploring the complex dynamics of tropical cyclone activity in the southern indian ocean: a multidecade analysis. *Jur. Penelit. Pendidik. IPA* **9**, 1069–1077 (2023).
22. Webster, P. J., Holland, G. J., Curry, J. A. & Chang, H. R. Changes in tropical cyclone number, duration, and intensity in a warming environment. *Science* **309**, 1844–1846 (2005).
23. Knutson, T. et al. Tropical cyclones and climate change assessment: part II: projected response to anthropogenic warming. *Bull. Am. Meteorol. Soc.* **101**, E303–E322 (2020).
24. Chan, J. C. & Liu, K. S. Global warming and western North Pacific typhoon activity from an observational perspective. *J. Clim.* **17**, 4590–4602 (2004).
25. Wu, L., Wang, B. & Braun, S. A. Implications of tropical cyclone power dissipation index. *Int. J. Climatol.* **28**, 727–731 (2008).
26. Lin, Y., Zhao, M. & Zhang, M. Tropical cyclone rainfall area controlled by relative sea surface temperature. *Nat. Commun.* **6**, 6591 (2015).
27. Kossin, J. P., Olander, T. L. & Knapp, K. R. Trend analysis with a new global record of tropical cyclone intensity. *J. Clim.* **26**, 9960–9976 (2013).
28. Wang, S. & Toumi, R. Recent migration of tropical cyclones toward coasts. *Science* **371**, 514–517 (2021).
29. Camargo, S. J. & Sobel, A. H. Western North Pacific tropical cyclone intensity and ENSO. *J. Clim.* **18**, 2996–3006 (2005).
30. Sattar, A. M. & Cheung, K. K. Comparison between the active tropical cyclone seasons over the Arabian Sea and Bay of Bengal. *Int. J. Climatol.* **39**, 5486–5502 (2019).
31. Malherbe, J., Engelbrecht, F. A. & Landman, W. A. Projected changes in tropical cyclone climatology and landfall in the Southwest Indian Ocean region under enhanced anthropogenic forcing. *Clim. Dyn.* **40**, 2867–2886 (2013).
32. Muthige, M. S. et al. Projected changes in tropical cyclones over the South West Indian Ocean under different extents of global warming. *Environ. Res. Lett.* **13**, 065019 (2018).

33. Sugi, M. & Yoshimura, J. Decreasing trend of tropical cyclone frequency in 228-year high-resolution AGCM simulations. *Geophys. Res. Lett.* **39**, L19805 (2012).

34. Sharmila, S. & Walsh, K. J. E. Recent poleward shift of tropical cyclone formation linked to Hadley cell expansion. *Nat. Clim. Change* **8**, 730–736 (2018).

35. Wang, B., Yang, Y., Ding, Q. H., Murakami, H. & Huang, F. Climate control of the global tropical storm days (1965–2008) *Geophys. Res. Lett.* **37**, L07704 (2010).

36. Kossin, J. P., Emanuel, K. A. & Vecchi, G. A. The poleward migration of the location of tropical cyclone maximum intensity. *Nature* **509**, 349–352 (2014).

37. Shan, K. & Yu, X. Enhanced understanding of poleward migration of tropical cyclone genesis. *Environ. Res. Lett.* **15**, 104062 (2020).

38. Zhan, R. & Wang, Y. Weak tropical cyclones dominate the poleward migration of the annual mean location of lifetime maximum intensity of northwest Pacific tropical cyclones since 1980. *J. Clim.* **30**, 6873–6882 (2017).

39. Lucas, C., Timbal, B. & Nguyen, H. The expanding tropics: a critical assessment of the observational and modeling studies. *Wiley Interdiscip. Rev.: Clim. Change* **5**, 89–112 (2014).

40. Waugh, D. W. et al. Revisiting the relationship among metrics of tropical expansion. *J. Clim.* **31**, 7565–7581 (2018).

41. Cao, X. et al. Westward shift of tropical cyclogenesis over the southern Indian Ocean. *Environ. Res. Lett.* **19**, 034016 (2024).

42. Holland, G. J. *Tropical Cyclone Motion: Environmental Interaction Plus A Beta Effect* (Colorado State Univ Fort Collins Dept of Atmospheric Science, 1982).

43. Chan, J. C. The physics of tropical cyclone motion. *Annu. Rev. Fluid Mech.* **37**, 99–128 (2005).

44. Landman, W. A., Seth, A. & Camargo, S. J. The effect of regional climate model domain choice on the simulation of tropical cyclone–like vortices in the southwestern Indian Ocean. *J. Clim.* **18**, 1263–1274 (2005).

45. Elsner, J. B., Kossin, J. P. & Jagger, T. H. The increasing intensity of the strongest tropical cyclones. *Nature* **455**, 92–95 (2008).

46. Emanuel, K. Evidence that hurricanes are getting stronger. *Proc. Natl Acad. Sci. USA* **117**, 13194–13195 (2020).

47. Malan, N., Reason, C. J. C. & Loveday, B. R. Variability in tropical cyclone heat potential over the Southwest Indian Ocean. *J. Geophys. Res.: Oceans* **118**, 6734–6746 (2013).

48. Chang-Seng, D. S. & Jury, M. R. Tropical cyclones in the SW Indian Ocean. Part 2: structure and impacts at the event scale. *Meteorol. Atmos. Phys.* **106**, 163–178 (2010).

49. Chan, J. C. An observational study of the physical processes responsible for tropical cyclone motion. *J. Atmos. Sci.* **41**, 1036–1048 (1984).

50. Tu, S., Chan, J. C., Xu, J. & Zhou, W. Opposite changes in tropical cyclone rain rate during the recent El Niño and La Niña years. *Geophys. Res. Lett.* **49**, e2021GL097412 (2022).

51. Tu, S., Zhang, Y., Liang, M., Wu, D. & Xu, J. Detecting the impact of climate change on tropical cyclones in Southern China. *Environ. Res. Lett.* **19**, 044067 (2024).

52. Mawren, D. & Reason, C. J. C. Variability of upper-ocean characteristics and tropical cyclones in the South West Indian Ocean. *J. Geophys. Res. Oceans* **122**, 2012–2028 (2017).

53. Fitchett, J. M. Recent emergence of CAT5 tropical cyclones in the South Indian Ocean. *South Afr. J. Sci.* **114**, 1–6 (2018).

54. Kuleshov, Y. et al. Trends in tropical cyclones in the South Indian Ocean and the South Pacific Ocean. *J. Geophys. Res. Atmos.* **115**, D01101 (2010).

55. Klotzbach, P. J. et al. Trends in global tropical cyclone activity: 1990–2021. *Geophys. Res. Lett.* **49**, e2021GL095774 (2022).

56. Mavume, A. F., Rydberg, L., Rouault, M. & Lutjeharms, J. R. Climatology and landfall of tropical cyclones in the south-west Indian Ocean. Western Indian Ocean. *J. Mar. Sci.* **8**, 15–35 (2009).

57. Kuleshov, Y. et al. Tropical cyclone genesis in the Southern Hemisphere and its relationship with the ENSO. *Ann. Geophys.* **27**, 2523–2538 (2009).

58. Ramsay, H. A., Camargo, S. J. & Kim, D. Cluster analysis of tropical cyclone tracks in the Southern Hemisphere. *Clim. Dyn.* **39**, 897–917 (2012).

59. Ho, C. H., Kim, J. H., Jeong, J. H., Kim, H. S. & Chen, D. Variation of tropical cyclone activity in the South Indian Ocean: El Niño-southern oscillation and madden-Julian oscillation effects. *J. Geophys. Res.: Atmospheres* **111**, D22101 (2006).

60. Astier, N., Plu, M. & Claud, C. Associations between tropical cyclone activity in the Southwest Indian Ocean and El Niño Southern Oscillation. *Atmos. Sci. Lett.* **16**, 506–511 (2015).

61. Chikoore, H., Vermeulen, J. H. & Jury, M. R. Tropical cyclones in the Mozambique channel: January–March 2012. *Nat. Hazards* **77**, 2081–2095 (2015).

62. Mao, R. et al. Is there a linkage between the tropical cyclone activity in the southern Indian Ocean and the Antarctic Oscillation? *J. Geophys. Res.: Atmos.* **118**, 8519–8535 (2013).

63. Hall, J. D., Matthews, A. J. & Karoly, D. J. The modulation of tropical cyclone activity in the Australian region by the Madden–Julian oscillation. *Mon. weather Rev.* **129**, 2970–2982 (2001).

64. Ash, K. D. & Matyas, C. J. The influences of ENSO and the subtropical Indian Ocean Dipole on tropical cyclone trajectories in the southwestern Indian Ocean. *Int. J. Climatol.* **32**, 41–56 (2012).

65. Werner, A., Maharaj, A. M. & Holbrook, N. J. A new method for extracting the ENSO-independent Indian Ocean Dipole: application to Australian region tropical cyclone counts. *Clim. Dyn.* **38**, 2503–2511 (2012).

66. Tridaiana, S., & Marzuki, M. Exploring ENSO and IOD effects on Southern Indian Ocean cyclones from 1970 to 2022. In *AIP Conference Proceedings* (Vol. 3116, No. 1). (AIP Publishing, 2024).

67. Mendelsohn, R., Emanuel, K., Chonabayashi, S. & Bakkensen, L. The impact of climate change on global tropical cyclone damage. *Nat. Clim. Change* **2**, 205–209 (2012).

68. Pillay, M. T. & Fitchett, J. M. Southern hemisphere tropical cyclones: a critical analysis of regional characteristics. *Int. J. Climatol.* **41**, 146–161 (2021).

69. Scoccimarro, E., Lanteri, P. & Cavicchia, L. Freddy: breaking record for tropical cyclone precipitation? *Environ. Res. Lett.* **19**, 064013 (2024).

70. Knapp, K. R., Kruk, M. C., Levinson, D. H., Diamond, H. J. & Neumann, C. J. The international best track archive for climate stewardship (IBTrACS) unifying tropical cyclone data. *Bull. Am. Meteorol. Soc.* **91**, 363–376 (2010).

71. Lu, D. et al. A rapid intensification warning index for tropical cyclones based on the analog method. *Geophys. Res. Lett.* **50**, e2022GL101951 (2023).

72. Zhong, Q., Li, J., Zhang, L., Ding, R. & Li, B. Predictability of tropical cyclone intensity over the western North Pacific using the IBTrACS dataset. *Mon. Weather Rev.* **146**, 2741–2755 (2018).

73. Hersbach, H. et al. The ERA5 global reanalysis. *Q. J. R. Meteorol. Soc.* **146**, 1999–2049 (2020).

74. Good, S. A., Martin, M. J. & Rayner, N. A. EN4: quality controlled ocean temperature and salinity profiles and monthly objective analyses with uncertainty estimates. *J. Geophys. Res.: Oceans* **118**, 6704–6716 (2013).

75. Tu, S. et al. Recent global decrease in the inner-core rain rate of tropical cyclones. *Nat. Commun.* **12**, 1948 (2021).

Acknowledgements

Author contributions

S.T. conceived and designed the study, S.T., Z.H., and M.L. conducted the data analyses, S.T. wrote the original draft. W.Z., J.X., and J.C.L.C. reviewed and edited the English writing of the paper. S.T., Z.H., M.L., W.Z., J.C.L.C., and J.X. discussed the results in the manuscript.

Competing interests

The authors declare no competing interest.

Additional information

Supplementary information The online version contains supplementary material available at
https://doi.org/10.1038/s43247-024-01683-2.

Correspondence and requests for materials should be addressed to Wen Zhou or Jianjun Xu.

Peer review information *Communications Earth & Environment* thanks the anonymous reviewers for their contribution to the peer review of this work. Primary Handling Editor: Alireza Bahadori. A peer review file is available.

Reprints and permissions information is available at
http://www.nature.com/reprints

Publisher's note Springer Nature remains neutral with regard to jurisdictional claims in published maps and institutional affiliations.